

Cubic C₂₀: An intrinsic superconducting carbon allotrope

Ying Yu¹, Xun-Wang Yan², Fengjie Ma³, Miao Gao^{1,4*}, and Zhong-Yi Lu⁵

¹Department of Physics, School of Physical Science and Technology, Ningbo University, Zhejiang 315211, China

²College of Physics and Engineering, Qufu Normal University, Shandong 273165, China

³The Center for Advanced Quantum Studies and Department of Physics, Beijing Normal University, Beijing 100875, China

⁴School of Physics, Zhejiang University, Hangzhou 310058, China

⁵Department of Physics, Renmin University of China, Beijing 100872, China

Finding intrinsic carbon superconductor is an interesting topic. Based on density functional first-principles calculations, we first study the phonon-mediated superconductivity in a cubic metallic carbon allotrope, namely sc-C₂₀, which has been synthesized in experiment. The electron-phonon coupling is accurately computed with Wannier interpolation method. By solving the Eliashberg equations, we predict that sc-C₂₀ is an intrinsic carbon superconductor, without introducing any guest atoms or doping, whose transition temperature is determined to be about 24 K. Our findings enrich the family of carbon-based superconductors.

The studies of carbon-based superconductor can be traced back to the 1960s. Superconductivity was first discovered in graphite intercalation compounds (GICs) below 1 K, such as KC₈.¹⁾ Under ambient pressure, the highest T_c for GICs is 11.5 K in CaC₆.²⁾ Graphene, the two-dimensional form of graphite, has gapless Dirac bands. Superconductivity in doped graphene has been extensively investigated.^{3–5)} Recently, correlated insulating states were observed in twisted bilayer graphene, and superconductivity emerges at 1.7 K after electrostatic doping.^{6,7)} For twisted trilayer graphene, rich phase diagram and better tunability of electric field were realized, compared with the bilayer case,^{8,9)} providing a fascinating playground to explore the interplay between correlated states and superconductivity. Insulator to superconductor transition was reported in boron-doped diamond,¹⁰⁾ in which the T_c exhibits a positive dependence on the proportion of boron that incorporated into diamond.¹¹⁾ It was found that the onset T_c of 27% boron-doped Q-carbon is 55 K.¹²⁾ Fullerene shows superconductivity at 18 K, after the potassium intercalation with stoichiometry of K₃C₆₀.¹³⁾ Subsequently, the T_c was improved to 33 K in RbCs₂C₆₀¹⁴⁾ and 40 K in Cs₃C₆₀.¹⁵⁾ Signatures of superconductivity were also detected in single- and multi-walled carbon nanotubes.^{16,17)} However, the superconductivity transition is quite sensitive to the configuration of Au electrode.¹⁷⁾ Organic compounds are possible candidates of carbon-based superconductors, such as K_{3,3}Picene,¹⁸⁾ but controversy still exists.¹⁹⁾

As what mentioned above, introducing guest atom or doping is inescapable to realize superconductivity in carbon materials. Therefore, it is quite interesting to know whether there is a carbon allotrope showing intrinsic superconductivity. To achieve this purpose, the first step is finding metallic carbon allotropes. K. Yamada prepared a cubic modification of carbon by shock compression method, with carbon black and tetracyanoethylene as starting materials.²⁰⁾ In the theoretical side, a simple cubic carbon, namely sc-C₂₀ [Fig. 1], was proposed.²¹⁾ The lattice constant of sc-C₂₀ is in excellent agreement with the synthesized cubic carbon. Moreover, by comparing the X-ray diffraction (XRD) patterns, it was found that most XRD peaks from the experiment can be interpreted through sc-C₂₀.²²⁾ Band structure calculation indicated that

sc-C₂₀ is metallic.²¹⁾ Besides sc-C₂₀, several metallic carbon allotropes were proposed theoretically, such as bct-4,²³⁾ T6-carbon,²⁴⁾ Hex-C₂₄,²⁵⁾ H₁₈ carbon,²⁶⁾ and C14-diamond.²⁷⁾ However, the electron-phonon coupling (EPC) and potential phonon-mediated superconductivity in all these metallic carbon allotropes have never been investigated so far. Two hypothetical sp^2 -hybridized carbons, namely GT-8 and GT-16 were suggested to be superconducting, with T_c being 5.2 K and 14.0 K, respectively.²⁸⁾ However, the evidences about their syntheses are not available. Very recently, different structural models were adopted to study the EPC and superconductivity of graphite-diamond hybrid, with predicted T_c ranging from 2 K to 42 K.²⁹⁾ Thus, the phase space of superconducting carbon allotrope needs to be further enriched.

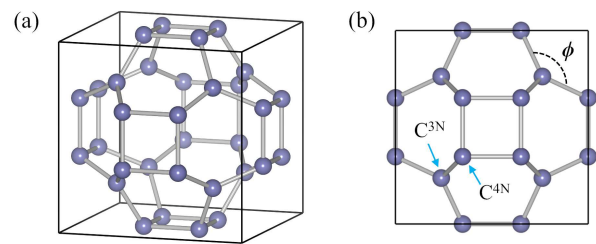


Fig. 1. (a) Three-dimensional view of the ball-stick model of sc-C₂₀. (b) View along the [001] direction. The solid black lines represent the cubic unit cell. C^{3N} and C^{4N} denote two nonequivalent carbon atoms. ϕ is the bond angle among sp^2 -bonded atoms. The ball-stick models are plotted with VESTA.³⁰⁾

Considering the fact that sc-C₂₀ has been synthesized, we perform the first-principles calculations of EPC and phonon-mediated superconductivity in sc-C₂₀. The atomic structure, elastic properties, electronic structure, phonons, isotropic Eliashberg spectral function, and evolution of superconducting gap versus temperature are systematically investigated in this work. As revealed by our calculations, the metallicity of sc-C₂₀ originates from the p orbitals of carbon atoms, which are perpendicular to the sp^2 -bonding planes. Phonon modes, including A_{2u} , T_{2g} , A_{1g} , E_g , and A_{2g} , involve in the EPC, providing multiple channels to pair electrons. The EPC constant

*gaomiao@nbu.edu.cn

λ and ω_{\log} are equal to 0.63 and 60.81 meV, respectively, giving rise to superconductivity with T_c being about 24 K. As a comparison, the EPC of other five carbon allotropes are also studied, including bct-4, T6-carbon, Hex-C₂₄, H₁₈ carbon, and C14-diamond. None of these compounds show superconductivity above 8 K.

Our density functional theory calculations were carried out based on the plane wave basis and pseudopotential methods. The Quantum-ESPRESSO package was adopted.³¹⁾ We calculated the electronic states and phonon perturbation potentials³²⁾ using the generalized gradient approximation of Perdew-Burke-Ernzerhoff (PBE) formula³³⁾ and the optimized norm-conserving Vanderbilt pseudopotentials.³⁴⁾ The kinetic energy cut-off and the charge density cut-off were set to 80 Ry and 320 Ry, respectively. A \mathbf{k} mesh of $18 \times 18 \times 18$ points in combination with a Methfessel-Paxton smearing³⁵⁾ of 0.02 Ry, was employed to calculate the self-consistent charge densities. Within the framework of density-functional perturbation theory,³⁶⁾ we computed the dynamical matrices and the perturbation potentials on a $6 \times 6 \times 6$ mesh. To construct the maximally localized Wannier functions of sc-C₂₀,³⁷⁾ we chose 36 hybridized σ states localized in the middle of carbon-carbon bonds and 8 s -type functions at the sp^2 -bonded carbon sites. The convergence of EPC constant λ was extensively checked through fine electron ($60 \times 60 \times 60$) and phonon ($20 \times 20 \times 20$) grids with the Electron-Phonon Wannier code.³⁸⁾ For the energy bands consistency between Wannier interpolation and first-principles calculations, the convergence test of EPC constant λ , and the spatial decay of electronic Hamilto-

nian in Wannier representation, please see the supplemental material.³⁹⁾ The Dirac δ -functions for electrons and phonons were smeared out by a Gaussian function with the widths of 20 meV and 0.5 meV, respectively. We determined the T_c by solving the isotropic Eliashberg equations. The sum over Matsubara frequencies was truncated with $\omega_c = 16$ eV, about 100 times that of the highest phonon frequency.

The crystal structure of sc-C₂₀ is shown in Fig. 1. Carbon atoms can be classified into two types. Eight sp^2 -bonded carbon atoms are seated close to the cell corners. Twelve sp^3 -hybridized carbon atoms locate around the face centers of the cubic cell, forming squares. According to the number of the nearest neighbors, these two nonequivalent carbon atoms are denoted as C^{3N} and C^{4N}, respectively [Fig. 1(b)]. sc-C₂₀ belongs to the space group $Pm\bar{3}m$ (No. 221). After optimization, the lattice constant of sc-C₂₀ is found to be 5.2135 Å, slightly larger than the one obtained by local density approximation (LDA).^{21,22)} C^{3N} and C^{4N} occupy 8g (0.2376, 0.2376, 0.2376) and 12i (0.0000, 0.3485, 0.3485) Wyckoff positions. The bond angle ϕ is 119.9° [Fig. 1(b)], indicating a perfect sp^2 hybridization, like in graphene. The mechanical stability of sc-C₂₀ is examined by calculating the elastic constants C_{ij} . For cubic crystals, there are only three independent C_{ij} coefficients, namely C_{11} , C_{12} , and C_{44} , which are determined to be 537.0 GPa, 224.2 GPa, and 228.1 GPa, respectively. It is known that the mechanical stability conditions for cubic systems are $C_{11} - C_{12} > 0$, $C_{11} + 2C_{12} > 0$, and $C_{44} > 0$,⁴⁰⁾ which are satisfied in sc-C₂₀. Using Voigt-Reuss-Hill approximation,⁴¹⁾ the bulk modulus B , shear modulus G , Young modulus E , and Poisson's ratio ν are 328.5 GPa, 196.1 GPa, 490.7 GPa, and 0.25, respectively. The elastic constants and bulk modulus are relatively smaller with respect to the LDA results,^{21,22)} due to the well-known overbinding problem of LDA. We also estimate the Vickers hardness of sc-C₂₀ with Chen's model,⁴²⁾ $H_v = 2(k^2 G)^{0.585} - 3$, in which the Pugh modulus ratio k equals G/B . sc-C₂₀ is not a superhard material with H_v of 21.0 GPa.

The electronic structure of sc-C₂₀ is presented in Fig. 2. It is clear that sc-C₂₀ is a metal, with two energy bands across the Fermi level [Fig. 2(a)]. Since PBE functional tends to underestimate the band gap, we also calculate the band structure using the hybrid functional HSE06.⁴³⁾ Although, a repulsion

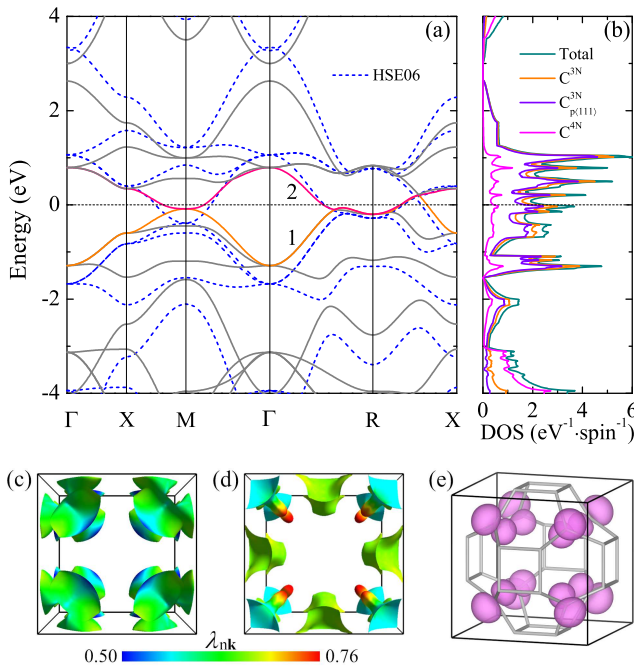


Fig. 2. Electronic structure for sc-C₂₀. (a) Band structure. The solid lines denote the PBE bands. The partially filled bands labeled as 1 and 2, are presented with different colors. The Fermi level is set to zero. (b) Total and partial density of states generated by PBE functional. (c)-(d) Fermi surfaces corresponding to band 1 and band 2, whereas the distribution of \mathbf{k} -resolved EPC constant $\lambda_{n\mathbf{k}}$ is shown. The FermiSurfer package is adopted.⁴⁴⁾ (e) Isosurface of charge density of strongly coupled electronic Kohn-Sham states drawn with VESTA.³⁰⁾ State at \mathbf{k} point ($\pm 0.26, \pm 0.26, \pm 0.26$) are included. The isovalue is set to 0.025 e/Bohr^3 .

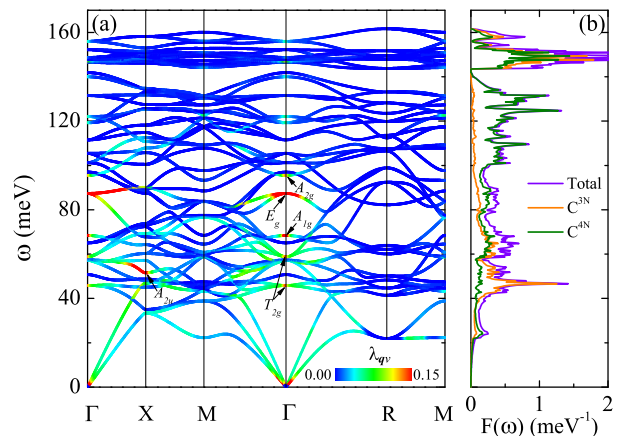


Fig. 3. Lattice dynamics of sc-C₂₀. (a) Phonon spectrum, colored by EPC constant $\lambda_{q\nu}$. (b) Total and projected phonon DOS $F(\omega)$.

effect is observed in comparison with the PBE bands. The HSE06 results resemble those of the PBE around the Fermi level. According to the partial density of states (DOS), C^{3N} atoms dominate the DOS from -3.0 eV to 3.0 eV [Fig. 2(b)]. Specifically, they contribute about 81.5% of the DOS at the Fermi level, i.e. $N(0)$. The p orbitals of C^{3N} that perpendicular to the sp^2 -bonding plane are along the $\langle 111 \rangle$ direction, which are denoted as $C^{3N}_{p\langle 111 \rangle}$. In particular, the DOS of C^{3N} almost originates from the $C^{3N}_{p\langle 111 \rangle}$ orbitals. Nevertheless, contribution of C^{4N} atoms mainly lies below -3.0 eV. The Fermi surfaces are shown in Fig. 2(c) and Fig. 2(d), with color mapping of the EPC strength λ_{nk} . All the pieces of the Fermi surfaces are close to the boundaries of Brillouin zone. The hotspots in Fig. 2(d) stand for the Kohn-Sham states that possess the strongest coupling with phonons. As confirmed by the charge distribution, these strongly coupled electronic states just correspond to the $C^{3N}_{p\langle 111 \rangle}$ orbitals [Fig. 2(e)].

Figure 3 shows the phonon spectrum and phonon DOS. Beside mechanical stability, sc- C_{20} is proved to be dynamically stable, as indicated by the phonon spectrum, whereas no imaginary phonon modes appear [Fig. 3(a)]. The symmetries of phonon modes which strongly couple with electrons are marked. For instance, the A_{2u} mode at X point, T_{2g} , A_{1g} , E_g , and A_{2g} modes at Γ point. The highest peak of phonon DOS is around 150 meV, originating from dispersionless modes [Fig. 3(b)]. These modes mix the movements of C^{4N} and C^{3N} atoms together, as demonstrated by the projected phonon DOS. The vibration of C^{4N} holds a dominant position from 80 meV to 140 meV. The situation is reversed below 60 meV.

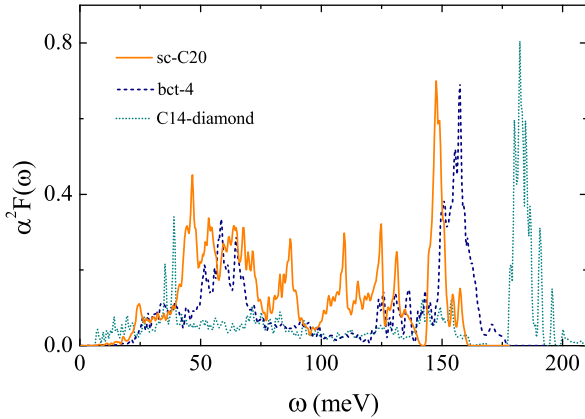


Fig. 4. Eliashberg spectral functions $\alpha^2 F(\omega)$ for sc- C_{20} , bct-4, and C14-diamond. The results of T6, Hex- C_{24} , and H_{18} carbon are not shown, due to weak EPC.

The Eliashberg spectral functions $\alpha^2 F(\omega)$ of sc- C_{20} , bct-4, and C14-diamond are given in Fig. 4. The multi-peak behavior of $\alpha^2 F(\omega)$ in sc- C_{20} naturally reflects the existence of various strongly coupled phonon modes, as uncovered in Fig. 3 (a). The peak near 150 meV is resulted from the large phonon DOS. In contrast, the reduced peak around 87 meV can be attributed to the limited DOS, although the E_g modes at Γ point have sizeable EPC strength. Compared with bct-4 and C14-diamond, two important features of $\alpha^2 F(\omega)$ are revealed for sc- C_{20} . On one hand, the phonons of sc- C_{20} ex-

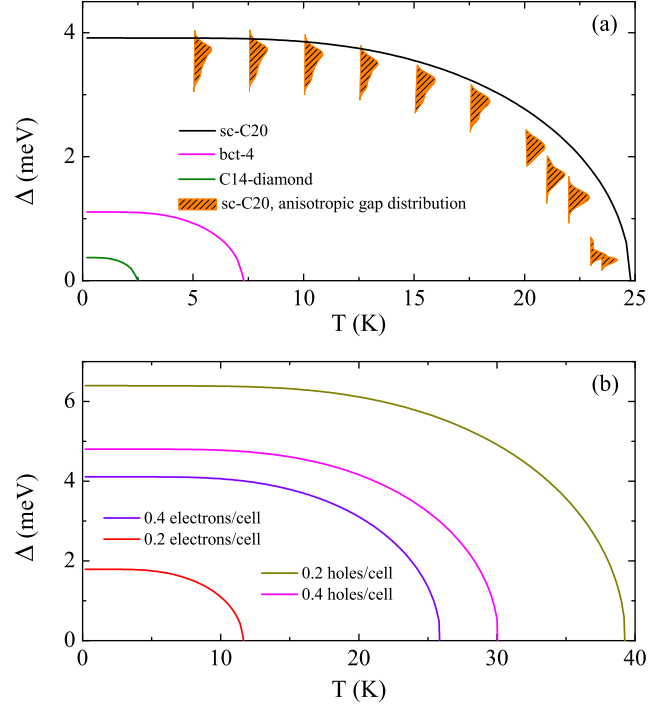


Fig. 5. (a) Superconducting energy gaps versus temperature for sc- C_{20} , bct-4, and C14-diamond, according to the results of isotropic Eliashberg equations. The shadowed yellow curve is the distribution of normalized superconducting energy gap generated by using the anisotropic Eliashberg equations. (b) T_c of doped sc- C_{20} . In our calculations, the screened Coulomb potential μ^* is set to 0.10.

hibit obvious softening, with the highest phonon frequency being about 160 meV, which is reduced by 23.0% with respect to that in C14-diamond. On the other hand, the spectral weight of $\alpha^2 F(\omega)$ of sc- C_{20} in the intermediate frequency range is significant, for example, from 80 meV to 120 meV. These two factors play vital roles in the enhancement of EPC in sc- C_{20} . The EPC constant λ and logarithmic average frequency ω_{\log} can be acquired through $\lambda = 2 \int \frac{\alpha^2 F(\omega)}{\omega} d\omega$, and $\omega_{\log} = \exp \left[\frac{2}{\lambda} \int \frac{d\omega}{\omega} \alpha^2 F(\omega) \ln \omega \right]$. We find that the EPC constants λ are 0.63, 0.42, 0.37, 0.16, 0.07, and 0.21 in sc- C_{20} , bct-4, C14-diamond, T6-carbon, Hex- C_{24} , and H_{18} carbon, respectively. The logarithmic average frequencies ω_{\log} are computed to be 60.81, 66.28, 47.10, 88.23, 111.60, and 72.18 meV, correspondingly.

In order to determine the T_c , the isotropic Eliashberg equations are solved self-consistently.^{45,46} The transition temperatures are calculated to be 24.6 K, 7.2 K, and 2.4 K, for sc- C_{20} , bct-4, and C14-diamond [Fig. 5(a)]. Close to zero temperature, the superconducting energy gaps are equal to 3.91, 1.11, and 0.37 meV, respectively. No superconducting transition occurs in T6-carbon, Hex- C_{24} , and H_{18} carbon. We also take the anisotropy of EPC into consideration. The superconducting energy gaps show visible anisotropy in sc- C_{20} . But the gap values group together, reflecting a single-gap nature. This can be rationalized by the fact that only one type orbital dominates the $N(0)$, i.e., $C^{3N}_{p\langle 111 \rangle}$. Moreover, the T_c is computed as 23.5 K, almost unaffected compared with the isotropic case. Considering the multiple-peak structure of DOS near the Fermi level [Fig. 2(b)], and the sensitivity

of T_c to $N(0)$, we further calculate the T_c of doped sc-C₂₀ to investigate its robustness against the change of $N(0)$. The doping concentrations are set to 0.4 electrons/cell, 0.2 electrons/cell, 0.2 hole/cell, and 0.4 hole/cell, respectively. Accordingly, we find that $N(0)$ equal to 3.34, 1.97, 3.46, and 3.01 states/spin/eV/cell, for above mentioned four doping cases, in comparison with 2.65 states/spin/eV/cell of pristine sc-C₂₀. After solving the isotropic Eliashberg equations, the transition temperatures are determined to be 25.8, 11.6, 39.2, and 30.0 K, respectively [Fig. 5(b)]. Although 0.2 electrons/cell doping leads to depressed T_c , doping holes can markedly boost the T_c . Our findings strongly suggest that sc-C₂₀ is a unique intrinsic superconducting carbon allotrope, with T_c even higher than most carbon-based superconductors.

In summary, we have investigated the phonon-mediated superconductivity in six carbon allotropes for the first time. The unpaired p orbitals that pointing to the corners of the cubic cell can account for the metallicity in sc-C₂₀. The symmetries of strongly coupled phonon modes are identified. Our calculations suggest that sc-C₂₀ is an outstanding intrinsic carbon superconductor. There is no need to introduce guest atoms or doping to realize superconductivity, unlike other carbon-based compounds. The transition temperature of sc-C₂₀ is higher than those in graphite intercalation compounds, and also comparable with respect to that predicted in graphite-diamond hybrid. The confirmation of its superconductivity in experiment is called for.

Acknowledgment

This work was supported by the National Natural Science Foundation of China (Grant Nos. 11974194, 11974207, 12074040, 11934020, and 11888101).

- 1) N. B. Hannay, T. H. Geballe, B. T. Matthias, K. Andres, P. Schmidt, and D. MacNair, *Phys. Rev. Lett.* **14**, 225 (1965).
- 2) N. Emery, C. Hérodol, M. d'Astuto, V. Garcia, Ch. Bellin, J. F. Marêché, P. Lagrange, and G. Loupias, *Phys. Rev. Lett.* **95**, 087003 (2005).
- 3) B. Uchoa and A. H. Castro Neto, *Phys. Rev. Lett.* **98**, 146801 (2007).
- 4) G. Profeta, M. Calandra, and F. Mauri, *Nat. Phys.* **8**, 131 (2012).
- 5) J. Chapman, Y. Su, C. A. Howard, D. Kundys, A. N. Grigorenko, F. Guinea, A. K. Geim, I. V. Grigorieva, and R. R. Nair, *Sci. Rep.* **6**, 23254 (2016).
- 6) Y. Cao, V. Fatemi, A. Demir, S. Fang, S. L. Tomarken, J. Y. Luo, J. D. Sanchez-Yamagishi, K. Watanabe, T. Taniguchi, E. Kaxiras, R. C. Ashoori, and P. Jarillo-Herrero, *Nature* **556**, 80 (2018).
- 7) Y. Cao, V. Fatemi, S. Fang, K. Watanabe, T. Taniguchi, E. Kaxiras, and P. Jarillo-Herrero, *Nature* **556**, 43 (2018).
- 8) Z. Zhu, S. Carr, D. Massatt, M. Luskin, and E. Kaxiras, *Phys. Rev. Lett.* **125**, 116404 (2020).
- 9) J. M. Park, Y. Cao, K. Watanabe, T. Taniguchi, and P. Jarillo-Herrero, *Nature* **590**, 249 (2021).
- 10) E. A. Ekimov, V. A. Sidorov, E. D. Bauer, N. N. Mel'nik, N. J. Curro, J. D. Thompson, and S. M. Stishov, *Nature* **428**, 542 (2004).
- 11) Y. Takano, T. Takenouchi, S. Ishii, S. Ueda, T. Okutsu, I. Sakaguchi, H. Umezawa, H. Kawarada, and M. Tachiki, *Diamond Relat. Mater.* **16**, 911 (2007).
- 12) A. Bhaumik, R. Sachan, S. Gupta, and J. Narayan, *ACS Nano* **11**, 11915 (2017).
- 13) A. F. Hebard, M. J. Rosseinsky, R. C. Haddon, D. W. Murphy, S. H. Glarum, T. T. M. Palstra, A. P. Ramirez, and A. R. Kortan, *Nature* **350**, 600 (1991).
- 14) K. Tanigaki, T. W. Ebbesen, S. Saito, J. Mizuki, J. S. Tsai, Y. Kubo, and S. Kuroshima, *Nature* **352**, 222 (1991).
- 15) T. T. M. Palstra, O. Zhou, Y. Iwasa, P. E. Sulewski, R. M. Fleming, and B. R. Zegarski, *Solid State Commun.* **93**, 327 (1995).
- 16) M. Kociak, A. Yu. Kasumov, S. Guéron, B. Reulet, I. I. Khodos, Yu. B. Gorbato, V. T. Volkov, L. Vaccarini, and H. Bouchiat, *Phys. Rev. Lett.* **86**, 2416 (2001).
- 17) I. Takesue, J. Haruyama, N. Kobayashi, S. Chiashi, S. Maruyama, T. Sugai, and H. Shinohara, *Phys. Rev. Lett.* **96**, 057001 (2006).
- 18) R. Mitsuhashi, Y. Suzuki, Y. Yamanari, H. Mitamura, T. Kambe, N. Ikeda, H. Okamoto, A. Fujiwara, M. Yamaji, N. Kawasaki, Y. Maniwa, and Y. Kubozono, *Nature* **464**, 76 (2010).
- 19) S. Heguri, M. Kobayashi, and K. Tanigaki, *Phys. Rev. B* **92**, 014502 (2015).
- 20) K. Yamada, *Carbon* **41**, 1309 (2003).
- 21) F. J. Ribeiro, P. Tangney, S. G. Louie, and M. L. Cohen, *Phys. Rev. B* **74**, 172101 (2006). sc-C₂₀ was also named as **tfg** in the Samara Carbon Allotrope Database, <http://sacada.sctms.ru>.
- 22) C. He, C. X. Zhang, H. P. Xiao, L. J. Meng, and J. X. Zhong, *Carbon* **112**, 91 (2017).
- 23) R. Hoffman, T. Hughbanks, M. Kertesz, and P. H. Bird, *J. Am. Chem. Soc.* **105**, 4831 (1983).
- 24) S. Zhang, Q. Wang, X. Chen, and P. Jena, *Proc. Natl. Acad. Sci. USA* **110**, 18809 (2013).
- 25) H. Bu, M. Zhao, W. Dong, S. Lu, and X. Wang, *J. Mater. Chem. C* **2**, 2751 (2014).
- 26) C.-X. Zhao, C.-Y. Niu, Z.-J. Qin, X. Ren, J.-T. Wang, J. Cho, and Y. Jia, *Sci. Rep.* **6**, 21879 (2016).
- 27) X. Wu, X. Shi, M. Yao, S. Liu, X. Yang, L. Zhu, T. Cui, and B. Liu, *Carbon* **123**, 311 (2017).
- 28) M. Hu, X. Dong, B. Yang, B. Xu, D. Yu, and J. He, *Phys. Chem. Chem. Phys.* **17**, 13028 (2015).
- 29) Y. Ge, K. Luo, Y. Liu, G. Yang, W. Hu, B. Li, G. Gao, X.-F. Zhou, B. Xu, Z. Zhao, and Y. Tian, *Mater. Today Phys.* **23**, 100630 (2022).
- 30) K. Momma and F. Izumi, *J. Appl. Crystallogr.* **44**, 1272 (2011).
- 31) P. Giannozzi, S. Baroni, N. Bonini, M. Calandra, R. Car, C. Cavazzoni, D. Ceresoli, G. L. Chiarotti, M. Cococcioni, I. Dabo, A. Dal Corso, S. de Gironcoli, S. Fabris, G. Fratesi, R. Gebauer, U. Gerstmann, C. Gougoussis, A. Kokalj, M. Lazzeri, L. Martin-Samos, N. Marzari, F. Mauri, R. Mazzarello, S. Paolini, A. Pasquarello, L. Paulatto, C. Sbraccia, S. Scandolo, G. Sclauzero, A. P. Seitsonen, A. Smogunov, P. Umari, and R. M. Wentzcovitch, *J. Phys.:Condens. Matter* **21**, 395502 (2009).
- 32) F. Giustino, M. L. Cohen, and S. G. Louie, *Phys. Rev. B* **76**, 165108 (2007).
- 33) J. P. Perdew, K. Burke, and M. Ernzerhof, *Phys. Rev. Lett.* **77**, 3865 (1996).
- 34) D. R. Hamann, *Phys. Rev. B* **88**, 085117 (2013).
- 35) M. Methfessel and A. T. Paxton, *Phys. Rev. B* **40**, 3616 (1989).
- 36) S. Baroni, S. de Gironcoli, A. Dal Corso, and P. Giannozzi, *Rev. Mod. Phys.* **73**, 515 (2001).
- 37) G. Pizzi, V. Vitale, R. Arita, S. Blügel, F. Freimuth, G. Granton, M. Gibertini, D. Gresch, C. Johnson, T. Koretsune, J. Ibañez-Azpiroz, H. Lee, J.-M. Lihm, D. Marchand, A. Marrazzo, Y. Mokrousov, J. I. Mustafa, Y. Nohara, Y. Nomura, L. Paulatto, S. Poncè, T. Ponweiser, J. Qiao, F. Thöle, S. S. Tsirkin, M. Wierzbowska, N. Marzari, D. Vanderbilt, I. Souza, A. A. Mostofi, and J. R. Yates, *J. Phys.: Condens. Matter* **32**, 165902 (2020).
- 38) S. Poncè, E. R. Margine, C. Verdi, and F. Giustino, *Comp. Phys. Commun.* **209**, 116 (2016).
- 39) Please see the supplemental material.
- 40) M. Born and K. Huang, *Am. J. Phys.* **23**, 474 (1955).
- 41) R. Hill, *Proc. Phys. Soc. A* **65**, 349 (1952).
- 42) X.-Q. Chen, H. Y. Niu, D. Z. Li, and Y. Y. Li, *Intermetallics* **19**, 1275 (2011).
- 43) J. Heyd, G. E. Scuseria, and M. Ernzerhof, *J. Chem. Phys.* **124**, 219906 (2006).
- 44) M. Kawamura, *Comp. Phys. Commun.* **239**, 197 (2019).
- 45) G. M. Eliashberg, *Sov. Phys. JETP* **11**, 696 (1960).
- 46) E. R. Margine and F. Giustino, *Phys. Rev. B* **87**, 024505 (2013).